Optical Engineering

OpticalEngineering.SPIEDigitalLibrary.org

Measuring resolution degradation of long-wavelength infrared imagery in fog

Brian J. Redman
John D. van der Laan
Karl R. Westlake
Jacob W. Segal
Charles F. LaCasse
Andres L. Sanchez
Jeremy B. Wright

SPIE.

Brian J. Redman, John D. van der Laan, Karl R. Westlake, Jacob W. Segal, Charles F. LaCasse, Andres L. Sanchez, Jeremy B. Wright, "Measuring resolution degradation of long-wavelength infrared imagery in fog," *Opt. Eng.* **58**(5), 051806 (2019), doi: 10.1117/1.OE.58.5.051806.

Optical Engineering 58(5), 051806 (May 2019)

Measuring resolution degradation of long-wavelength infrared imagery in fog

Brian J. Redman,[a,b] John D. van der Laan,[a] Karl R. Westlake,[a] Jacob W. Segal,[a] Charles F. LaCasse,[a] Andres L. Sanchez,[a] and Jeremy B. Wright[a,*]
[a]Sandia National Laboratories, Albuquerque, New Mexico, United States
[b]University of Arizona, College of Optical Sciences, Tucson, Arizona, United States

Abstract. The scattering of light in fog is a complex problem that affects imaging in many ways. Typically, imaging device performance in fog is attributed solely to reduced visibility measured as light extinction from scattering events. We present a quantitative analysis of resolution degradation in the long-wave infrared regime. Our analysis is based on the calculation of the modulation transfer function from the edge response of a slant edge blackbody target in known fog conditions. We show higher spatial frequencies attenuate more than low spatial frequencies with increasing fog thickness. These results demonstrate that image blurring, in addition to extinction, contributes to degraded performance of imaging devices in fog environments. [DOI: 10.1117/1.OE.58.5.051806]

Keywords: degraded visual environments; modulation transfer function; infrared imaging; scattering; long-wavelength infrared; fog.

Paper 181265SS received Sep. 5, 2018; accepted for publication Dec. 12, 2018; published online Jan. 12, 2019.

1 Introduction

Fog is perhaps the most concerning degraded visual environment because it occurs in all climates and has significant effects on transportation and security. Fog remains a major problem for transportation[1,2] and with the increase in autonomous drivers it could become an even more dangerous issue. Remarkably, fog was the second highest cause of aviation accidents after wind in 2016.[3] Aviation accidents occur because fog causes a significant reduction in the visual acuity of pilots and tower crews creating dangerous operating conditions.[4] The use of digital imaging systems holds many advantages that may ultimately overcome the challenges of seeing in fog. One advantage is to use wavelengths of light that are not perceptible to the human eye. The long-wavelength infrared (LWIR) waveband is of particular interest because long wavelength light is less affected by scattering. However, LWIR is still scattered by fog due to the relation of the particle size and the wavelength. In order to improve safety and security, it is important to understand exactly how scattering from fog degrades imagery. In this paper, we present experimental results that quantitatively reveal how scattering from fog not only reduces the number of collected photons but also how the resolution of LWIR imagery is reduced.

Image degradation from fog is caused by three factors as determined by Mie theory:[5] extinction, increased background light,[6] and image blurring[7] Extinction is caused by a combination light scattering beyond the acceptance angle of the imaging system and absorption along the optical path and degrades all spatial frequencies equally. Increased background light is caused by unwanted ambient light being scattered toward the imaging system and increases the zero-frequency component of the image thereby reducing the contrast of all spatial frequencies. Image blurring is caused by photons that arrive at the detector offset from where they originate in a scene and degrades high spatial frequencies more than low spatial frequencies.

Previous work[8–14] has explored how extinction from fog affects LWIR image quality. To date, few experimental results have quantified the image blurring of the LWIR waveband through fog. Akopdjanan et al.[8] experimentally showed qualitative differences between visible, short-wave infrared, and LWIR scenes taken from an aircraft during clear and foggy conditions. Akopdjana's results indicated that the LWIR image quality was greatly reduced by both extinction and blurring. Beier et al.[11] simulated the loss of visibility in the LWIR waveband due to fog. Additionally, they compared simulations to measurements of transmission from point sources through naturally occurring fogs over several days. Beier et al. used the visibility metric of transmission, defined by the Koschmieder formula:

$$V = -\frac{\ln(0.05)}{\beta}, \tag{1}$$

where V was the visibility in meters and β was the extinction coefficient of the environment in inverse meters. Beier et al.'s results showed that LWIR visibility was dependent on the particle sizes of the fog. Gultepe et al.[15,16] showed that visibility is better correlated to the droplet concentration and liquid water content (LWC) of fog than to just the particle sizes. Beier and Gemperlein[10] performed simulations to compare the effectiveness of infrared and visible imaging systems for assisting aircraft landings. Simulated scenes were attenuated based on MODTRAN absorption models for fog. They selected a MODTRAN particle size distribution for the desired climate, and increased droplet concentration until the visibility for 550-nm light dropped to match the International Civil Aviation Organization (ICAO) range categories: 1220 m for CAT I, 610 m for CAT II, 305 m for CAT IIIa, and 92 m for CAT IIIc. It should be noted that

*Address all correspondence to Jeremy B. Wright, E-mail: jbwrigh@sandia.gov

MODTRAN accounts for extinction but does not account for other factors such as increased background light or image blurring caused by scattering. A detector model was applied to the attenuated scene to determine which wavelength band would perform best for the considered task. These simulations showed that for CAT I (no fog) and II (thin fog) LWIR cameras had a longer detection range than visible or mid-wave infrared cameras. In contrast, the LWIR waveband did not offer any improvement for CAT III (thick fog). Dumoulin and Boucher[12] created absorption models to correct remote temperature measurements made using LWIR cameras during foggy conditions. The absorption models were tested in an enclosed fog environment. Dumoulin et al.'s experimental results showed there is a nonlinear difference between visibility measured by a 550-nm wavelength transmissometer and the visibility measured from an extended visible and LWIR source through generated fog. The difference between the transmissometer measurement and the visibility measurement from extended sources illustrated a more complex relationship between a visibility metric and the appearance of a target.

Image blurring degrades the high-frequency information, which is important for identification tasks. The resolution loss caused by scattering in aerosols and fog has been well-studied for visible light.[1,6,7,13,15–23] Some of the studies determined the effect of image blurring was negligible.[13,21,22] However, other studies demonstrated that image blurring significantly decreased image quality.[7,17–20,23] Sadot et al.[24] showed that scattering from aerosols significantly affected LWIR image quality in clear conditions. The previous measurements[10–12,14] of LWIR imaging performance through fog did not account for the resolution degradation cause by blurring. We seek to expand upon this previous work with experimental results that quantitatively show how fog blurs LWIR imagery. In this paper, we utilize the modulation transfer function (MTF) of an LWIR imaging system through a wide range of fog thicknesses to demonstrate the image blurring effect caused by fog.

2 Experiment

Our experiment consisted of an LWIR camera and a blackbody target in a fog chamber to measure image degradation. We used a generated fog because it allowed for more controlled and repeatable measurements. A repeatable, well-characterized, atmospheric analogue[25] was generated in the Sandia National Laboratories fog facility. The facility was an enclosed 3 m × 3 m × 55 m chamber. This capability was demonstrated in previous studies that show resolution degradation caused by fog in visible imaging systems[23] and how polarized light was transmitted in fog.[26]

Sandia's fog facility generates an aerosol by spraying a salt water solution through 80 spray nozzles distributed along the length of the chamber. The salt makes the water droplets more hygroscopic, which increases the mean radius of the particle size distribution[25] The dissolved salt does not appreciably change the refractive index of the droplets, therefore, the optical properties of the fog are not directly dependent on the salt concentration. The ambient temperature can also be varied to change the particle size distribution of the fog. The temperature of the facility ranges from 16°C to 25°C. After the fog is generated, natural dissipation decreases the concentration of water in the air, which also decreases the optical thickness of the fog. The fog is well characterized, as described below, so that measurement parameters can be correlated with fog properties instead of time.

To characterize the fog, we used a Spraytec™ laser diffraction particle sizer from Malvern Instruments®, and an in-house transmissometer. Both instruments collected data at a rate of 1 Hz. The Spraytec measured the particle size distribution of the fog by drawing particles through a laser beam and measuring the diffraction pattern with a proprietary detector array.[27] This instrument can size particles with diameters from 0.1 to 2000 μm. The transmissometer measured the transmission over a fixed distance of fog with a 543-nm green HeNe laser and a detector with a small angular collection. The transmitter and receiver separation was set to 6.1 m for this experiment. Transmission values were calculated by taking the ratio of the measured radiant flux in fog to a baseline measurement without fog.

Meteorological optical range (MOR) is calculated by utilizing the transmissometer measured transmission data. MOR avoids the ambiguity between the colloquial visibility, which is a qualitative measure based on the distance that a person can see an object, and quantitative visibility which is a measure of extinction used by the studies cited in the introduction. Additionally, MOR is relatively available with meteorological data. MOR is defined as "the length of path in the atmosphere required to reduce the luminous flux in a collimated beam from an incandescent lamp, at a color temperature of 2700 K, to 5 percent of its original value, the luminous flux being evaluated by means of the photometric luminosity function of the International Commission on Illumination.[28] For the remainder of this paper we use an equivalent of MOR where the absorption is measured at 543 nm to match our transmissometer instead of integrated over a 2700-K broadband blackbody spectrum. The Beer–Lambert law is used to calculate the distance that the radiant flux is reduced to 5% of its initial value. The Beer–Lambert law

$$\Phi = \Phi_0 e^{-\beta L}, \tag{2}$$

where Φ is the flux through the fog, and Φ_0 is the flux without fog, β is the extinction coefficient, and L is the optical path length, describes how light is attenuated through an absorbing and or scattering media. The MOR, from the above definition, is the distance where Φ is 5% of Φ_0 therefore,

$$\mathrm{MOR} = \frac{-\ln(0.05)}{\beta}. \tag{3}$$

It is generally not feasible to move the detector along the beam to find a distance, so β is calculated for a fixed distance:

$$\beta = -\ln\left(\frac{\Phi}{\Phi_0}\right)\frac{1}{L}. \tag{4}$$

The equation used to compute the MOR is calculated by combining Equations (3) and (4):

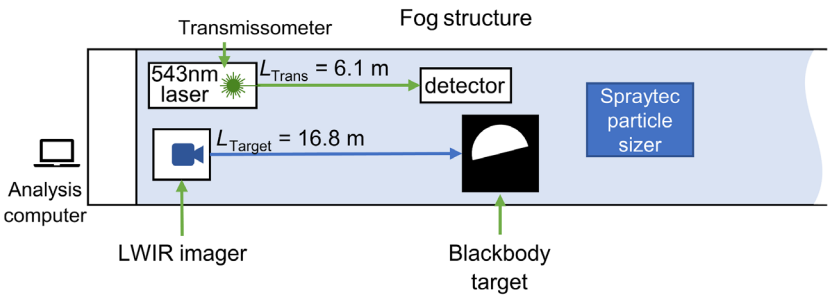

Fig. 1 Experimental setup: A 0.5 m × 0.5 m blackbody target was set 16.8 m away from an LWIR camera. The camera was housed in a positive pressure dry box to place the camera directly in the fog and minimize any nonuniformities. The chamber is sealed with double doors so that the fog will naturally dissipate instead of diffusing out of the chamber. The total chamber length is 55 m.

$$\mathrm{MOR}_{543} = L_{\mathrm{trans}} \frac{\ln(0.05)}{\ln\left(\frac{\Phi}{\Phi_0}\right)}, \tag{5}$$

where MOR_{543} is the MOR equivalent in meters, L_{trans} is the distance between the source and the detector of the transmissometer, Φ is the flux on the detector, and Φ_0 is the initial flux.

The Spraytec and transmissometer directly measure particle size distribution and transmission, but these parameters can be used to calculate parameters typically presented in the literature characterizing fog. LWC, which is defined as the mass of water in a volume of air,[1] can be calculated using the transmission from the transmissometer and the particle size distribution from the Spraytec[27,29] as follows:

$$\mathrm{LWC} = \frac{-2\ln\left(\frac{\Phi}{\Phi_0}\right)}{3L_{\mathrm{trans}}\sum_i \frac{Q_i(d_i)v_i}{d_i}}\rho_{\mathrm{water}}, \tag{6}$$

where Φ is the flux measured by the transmissometer through the fog, Φ_0 is the flux without fog, $Q(d)$ is the unitless extinction coefficient calculated from Mie theory for a sphere of water with a given diameter, v_i is the percentage of the total volume contributed by particles with diameter d_i, L_{trans} is the optical path length of the transmissometer, and ρ_{water} is the density of water (approximated as 1 g/cm^3 for this paper). We used the transmission from the transmissometer in the liquid water calculation instead of the transmission from the Spraytec because the longer distance improves accuracy. The Spraytec manual[27] contains the derivation for calculating the volume concentration which can be converted to LWC using the density of water.

Another parameter, which is related to the transmission and particle size distribution of fog, is the droplet concentration (N_d). The parameter N_d can be calculated by dividing the LWC into the volumes of individual particles:

$$N_d = \frac{\mathrm{LWC}}{\rho_{\mathrm{water}}}\sum_i \frac{3v_i}{4\pi r_i^3}. \tag{7}$$

Gultepe et al.[6] showed that the MOR was strongly correlated with the one over the product of LWC and N_d. These parameters have an added benefit that they can be estimated as part of meteorological simulations.

Figure 1 shows a schematic of our experimental setup to measure the LWIR resolution, which consisted of an FLIR® Tau™ 2 microbolometer viewing a slant edge target. The slant edge target consisted of a metal plate with a half-moon cutout placed in front of a 0.5 m × 0.5 m blackbody. The surface facing toward the black body is polished to minimize absorption, and the surface toward the camera has a high-emissivity coating to release absorbed heat and to avoid stray reflections. The blackbody was set to 37°C to approximate the temperature of the human body.

The FLIR® Tau™ 2 is an uncooled microbolometer with a resolution of 640 × 512 pixels with a pixel pitch of 17 μm. It is sensitive to wavelengths from 7.5 to 13.58 μm. Our optical assembly included a 100-mm focal length $F/1.6$ lens. We recorded 14-bit images in 15 frame bursts at 30 Hz that were separated by 3 s. Each burst was averaged to reduce the noise in the image. Data collection started 1 min before the beginning of fog generation in order to get a baseline frequency response as seen in Fig. 2(a). All measurements were referenced to this baseline.

A single fog test consisted of a 22-min conditioning spray to raise the humidity in the chamber and generate a thick fog. The fog dissipated naturally until the transmission was 20% as measured by the transmissometer. Following the conditioning spray, additional sprays were performed to further increase the optical thickness of the fog. Our ability to control the optical thickness of the fog allowed measurements of imaging performance over fine steps of fog optical thickness. Figure 2 shows example images and particle size distributions at a few representative fog optical thicknesses.

Our particle size distributions match the results of Arnulf et al.,[9] however, MODTRAN models for advection fogs[30] and other measured natural fogs have much larger particles. Mie theory predicts that as the particle size increases the light will be preferentially forward scattered into a smaller angle. The smaller scattering angle will result in the imaging system collecting more scattered photons resulting in more image blurring. The decreased scattering because the particles are much smaller than the wavelength also explains why the features of the target can be discerned at distances much greater than the MOR.

The fog generated in Sandia's fog facility is much thicker than naturally occurring fog allowing us to approximate longer viewing distances. Using optical thickness (τ) and the Beer–Lambert law, we can determine the equivalent distance for a thinner natural fog. The optical thickness is defined as the product of the extinction coefficient and optical path length from Eq. (2):

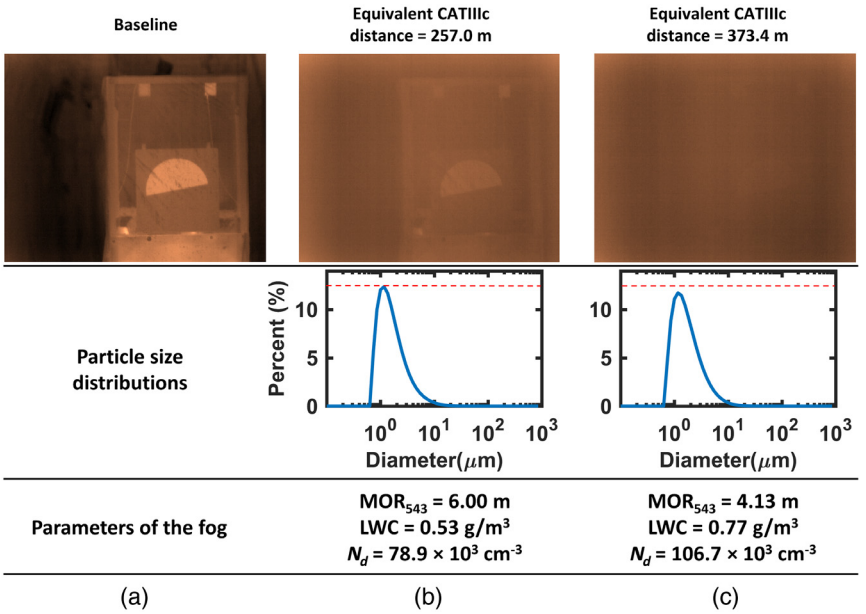

Fig. 2 Image degradation example images with various fog optical thicknesses and associated fog parameters. The parameters are MOR, LWC, and droplet concentration (N_d). (a) Baseline image without fog. All the measurements were referenced to these results. (b) The impact on spatial resolution of imaging through a fog with a MOR_{543} of 6.00 m, which is equivalent to a target distance of 257.0 m through a fog with an MOR of 92 m. (c) Image showing that the region around the target is brighter than the surrounding scene, but the details of the target are obscured. The blurred-out image indicates that the low spatial frequencies are attenuated less than the high spatial frequencies.

$$\tau = \beta L. \tag{8}$$

For the case of scattering, the optical thickness is defined as follows:

$$\tau = \rho \sigma L, \tag{9}$$

where ρ is the density of particles in units of particles per volume (this is equivalent to droplet number concentration, N_d), σ is the extinction cross section in units of area, and L is the optical path length. Equation (9) shows that halving the optical path length and doubling the concentration of the particles results in an equivalent optical thickness. The optical thickness between the source and detector of the transmissometer was calculated using

$$\tau_{\text{trans}} = -\ln\left(\frac{\Phi}{\Phi_0}\right). \tag{10}$$

We assume that the density and cross section of the fog are uniform throughout the facility. This allows us to use Eq. (9) to calculate the optical thickness between the LWIR image and the target as follows:

$$\tau_{\text{target}} = \frac{\tau_{\text{trans}}}{L_{\text{trans}}} L_{\text{target}}, \tag{11}$$

where L_{trans} is the distance between the transmissometer source and detector, and L_{target} is the distance between the camera and the target. Combining Eqs. (5) and (10), the MOR is defined as

$$\text{MOR} = -\frac{\ln(0.05)}{\tau} L, \tag{12}$$

which is a property of the fog independent of the measurement distances. As mentioned at the start of this discussion, the particle concentrations of the generated fog are much greater than naturally occurring fog. To show the equivalent effect of scattering in thinner fogs, we convert fog thicknesses to target distances using Eq. (12) with a constant thickness:

$$L_{\text{equivalent}} = \frac{\text{MOR}_{\text{equivalent}}}{\text{MOR}_{\text{generated}}} L_{\text{target}}. \tag{13}$$

As an example, Table 1 shows the distance through a thick naturally occurring fog to have the same extinction as the measurements made in this paper. For the thick naturally occurring fog, we chose an MOR equal to 92 m. This MOR value corresponds to a fog with the least extinction that still falls under the ICAO's thickest visual range category, CAT IIIc.

3 Analysis

A useful tool for describing the frequency dependence on the optical system is the MTF. The MTF is a normalized metric often used to test lens designs[31] that describes how spatial frequencies are degraded between the scene and the detector of an optical system. In this experiment, the MTF directly describes how fog affects the spatial information in a given image.

An intuitive understanding of the MTF can be described by observing at an image of a sharp black to white edge. The sharpness of the edge remains the same if the all the values in the image are divided by a constant value or a constant value is added to the entire image. In both cases, the image contrast is decreased while the edge sharpness remains constant. High spatial frequencies are required to resolve the sharp edge.

Table 1 To give context for the distances and optical thicknesses presented in this paper, we convert the optical thickness (τ) of our generated fog to equivalent target distances through a fog with MOR equal to 92 m. 92 m was chosen because it corresponds to the upper bound of the ICAO's thickest fog category, CAT IIIc.

Example case	Fog facility MOR (m)	Target distance (m)	τ	MOR of CAT IIIc (m)	Equivalent CAT IIIc distance
Thinnest fog presented in this paper	11.25	16.8	4.47	92	137 m
Fig. 2(b)	6.00	16.8	8.38	92	258 m
Fig. 2(c)	4.13	16.8	12.20	92	374 m
Thickest fog presented in this paper	3.20	16.8	15.70	92	515 m
Full length of facility	3.20	55.0	51.50	92	1580 m

When high frequencies are degraded, the edge will round off in an image blurring effect. The ratio of the imaging system's high-frequency response to low-frequency response gives a metric for describing the sharpness of the edge in the final image. This example of using a sharp edge to measure the frequency response of an optical system illustrates how the MTF is calculated from an edge response.[32] This measurement technique is used for the analysis of our experimental results.

The MTF is well suited for characterizing image blurring caused by scattering. Signal loss from scattering and absorption is caused by extinction, increased background light, and image blurring. The normalization of the MTF removes constant attenuation across all frequencies caused by extinction. Additionally, the technique to calculate the MTF uses a derivative, which removes the constant offset added to an image from increased background light. The blurring effect will reduce high frequencies more than low frequencies, which will change the frequency dependence of the MTF.

To calculate the MTF from the slant edge target, the edge response function (ERF) must be converted to a line spread function (LSF), which is a one-dimensional impulse response of the system. The Fourier transform of an impulse response gives the frequency response of the system. Figure 3 shows example data for each step in the following derivation. The LSF is the derivative of the ERF, a direct conversion is thus a numerical derivative. Numerical derivatives amplify noise, so instead we utilize the method proposed by Tzannes, et al.[32,33] Three Fermi functions are fit to the transition of the slant edge as follows:

$$\mathrm{ERF}(x) = D + \sum_{n=0}^{2} \frac{a_n}{e^{(x-b_n)\,c_n} + 1}, \tag{14}$$

where x is the distance perpendicular to the edge of each pixel that is being fit, and D, a, b, and c are the fitting parameters. With the functional form of the ERF, an analytic derivative can be calculated that does not amplify the noise. This derivative is the LSF defined as

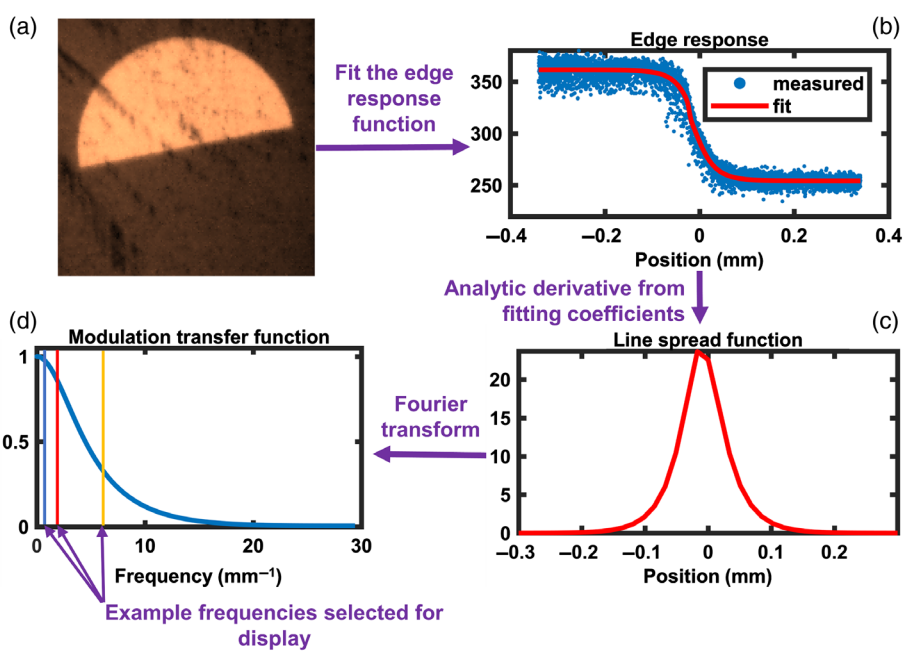

Fig. 3 MTF calculation from a slant edge target example. (a) Example image of the slant edge target and (b) ERF and the sigmoidal function fit. (c) The LSF calculated from the fitting coefficients. (d) The MTF is the magnitude of the Fourier transform the LSF. The example frequencies are marked to show how they relate to the entire MTF.

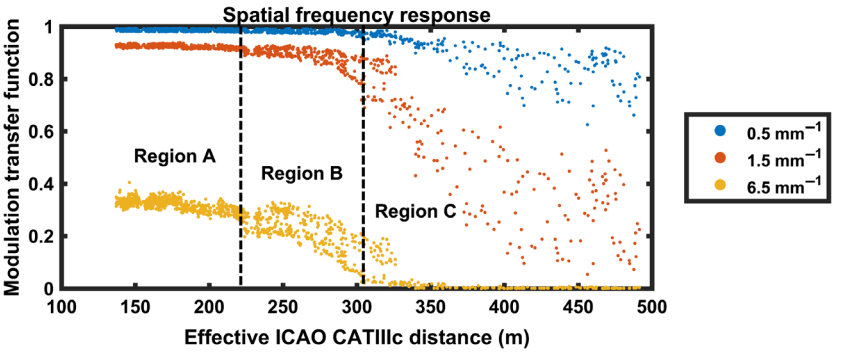

Fig. 4 Representative frequencies of the MTF show how high spatial frequencies are attenuated relative to low spatial frequencies over a range of effective distances through a fog with an MOR of 92 m. The effective distance was calculated by converting MOR to imaging distance using Eq. (13). The MTF is divided into regions to illustrate different slopes. In region A, the MTF has a slight change with increasing effective distance. In region B, the 6.5-mm^{-1} frequency is attenuated sharply with increasing effective distance, and the 1.5-mm^{-1} frequency is noticeably attenuated with increasing distance. In region C, the 6.5-mm^{-1} frequency information is effectively not measurable, and both of the lower frequencies are attenuated sharply with increasing target distance.

$$\mathrm{LSF}(x') = \left|\frac{\mathrm{ERF}(x')}{\mathrm{d}x}\right| = \left|\sum_{n=0}^{2} \frac{a_n c_n e^{(x'-b_n)c_n}}{[e^{(x'-b_n)c_n}+1]^2}\right|, \tag{15}$$

where x' is a vector of distances with the same sample separation as the pixel pitch of the detector. The derivative also removes the constant term. The x' vector was empirically chosen to be 4096 elements to oversample the MTF. The Fourier transform of the LSF is a slice out of the 2-D MTF. The MTF is then defined as

$$\mathrm{MTF}(\xi) = |\mathcal{F}_{x'\to\xi}[\mathrm{LSF}(x')]|, \tag{16}$$

where ξ is the spatial frequency in image space coordinates, and $\mathcal{F}_{x'\to\xi}$ is the discrete Fourier transform operator. This technique calculates the MTF for each of our averaged experimental frames. For the discussion, we chose three representative frequencies to illustrate how the MTF changes with fog optical thickness. Also the optical thicknesses of the fog were converted to effective target distances for a fog with an MOR of 92 m.

4 Results

To show how the blurring effect degrades image quality over a range of fog optical thicknesses, we plotted three representative frequencies from the MTF for two fog generation–dissipation cycles. The transmission of the fog was used to calculate the MOR_{543}. However, for the very thick fogs measured in this experiment, the MOR_{543} varied from 3.20 to 11.25 m. To present the data with a more useful metric, we used Eq. (13) to convert MOR_{543} to target distances through a fog with a fixed MOR_{543} equal to 92 m. The optical thickness was maintained by doubling the viewing distance and halving the particle concentration. The MOR_{543} of 92 m was selected because it corresponds to the thinnest fog that falls under the ICAO's thickest fog category, CATIIIc. Figure 4 shows the example frequencies from the MTF versus effective distance.

The MTF versus effective distance is divided into three regions to guide the discussion of the data. For region A (effective distance from 137 to 220 m), the MTF changes little, meaning that there is little blurring effect in this region. However, in region B (effective distance from 220 to 300 m), the response of the 6.5 mm^{-1} frequency decreases sharply with increasing effective range. There are also two clusters in the data corresponding to the separate generation–dissipation cycles. The separation in region B indicates that even slight differences in the composition of the fog have a significant effect on how the fog degrades spatial frequency, even for the same extinction. The response of the 1.5-mm^{-1} frequency decreases slightly with increasing effective distance in region B, whereas the response of the 0.5-mm^{-1} frequency is nearly unaffected. In region C (effective distance >300 m), the 6.5-mm^{-1} frequency is effectively not measurable, whereas the response of the 1.5-mm^{-1} frequency sharply decreases with the increasing effective target distance. Even the response of the 0.5-mm^{-1} frequency is degraded with increasing effective distance in region C.

These results show that in highly scattering fogs, the scattering changes the frequency response of the system in a more complex way than the simple extinction model suggests. The results presented show the spatial frequency-dependent degradation for fogs that are of concern for the transportation industry in CAT IIIc fogs. For future work, we plan to investigate how particle size affects the frequency response and causes the clustering in region B for the 6.5-mm^{-1} frequency.

5 Conclusions

We have shown that the blurring effect from scattering when imaging through optically thick fogs is an important consideration for the LWIR waveband. We show that higher spatial frequencies drop off in thinner fogs and are cutoff at optical thicknesses of fog that do not significantly degrade low spatial frequencies. The preferential degradation of high spatial frequencies over low spatial frequencies demonstrates that there is image quality degradation from blurring in addition to degradation from extinction and increased background light. The results presented here show that blurring is not significant over the spatial frequency range measured by our experiment for thin fog. Understanding how fog affects image quality is important for improving the ability to design instruments to see through fog. Ignoring image blur caused by fog and relying solely on traditional descriptions such as visibility results in the overestimation of image quality for

a given fog condition. Combining the MTF and metrics such as visibility to describe the overall image degradation of a given fog provides a more complete description of imaging through fog.

Acknowledgments

We thank Dylan Anderson for the useful discussions, Steven Storch and Taylor Settecerri for their work operating the fog facility, Joe Wolfgang from Malvern Instruments for technical assistance, and Dr. David Scrymgeour for organizing the project. Sandia National Laboratories is a multimission laboratory managed and operated by the National Technology and Engineering Solutions of Sandia, LLC, a wholly owned subsidiary of Honeywell International Inc., for the U.S. Department of Energy's National Nuclear Security Administration under Contract No. DE-NA0003525. This paper describes objective technical results and analysis. Any subjective views or opinions that might be expressed in the paper do not necessarily represent the views of the U.S. Department of Energy or the United States Government.

References

1. I. Gultepe et al., "Fog research: a review of past achievements and future perspectives," *Pure Appl. Geophys.* **164**(6), 1121–1159 (2007).
2. P. A. Pisano, L. C. Goodwin, and M. A. Rossetti, "US highway crashes in adverse road weather conditions," in *24th Conf. on Int. Interactive Information and Processing Systems for Meteorology, Oceanography and Hydrology, New Orleans, LA* (2008).
3. A. J. Fultz and W. S. Ashley, "Fatal weather-related general aviation accidents in the United States," *Phys. Geogr.* **37**(5), 291–312 (2016).
4. J. McCreary et al., "Human factors: Tenerife revisited," (1998).
5. C. F. Bohren and D. R. Huffman, *Absorption and Scattering of Light by Small Particles*, John Wiley & Sons, New York (2008).
6. I. Gultepe et al., "The fog remote sensing and modeling field project," *Bull. Am. Meteorol. Soc.* **90**(3), 341–360 (2009).
7. N. S. Kopeika, I. Dror, and D. Sadot, "Causes of atmospheric blur: comment on Atmospheric scattering effect on spatial resolution of imaging systems," *J. Opt. Soc. Am. A* **15**(12), 3097–3106 (1998).
8. Y. A. Akopdjanan et al., "Flight study of on-board enhanced vision system for all-weather aircraft landing," in *20th Int. Symp. on Atmospheric and Ocean Optics: Atmospheric Physics*, Vol. 6 (2014).
9. A. Arnulf et al., "Transmission by haze and fog in the spectral region 0.35 to 10 microns*," *J. Opt. Soc. Am.* **47**(6), 491–498 (1957).
10. K. Beier and H. Gemperlein, "Simulation of infrared detection range at fog conditions for enhanced vision systems in civil aviation," *Aerosp. Sci. Technol.* **8**(1), 63–71 (2004).
11. K. R. Beier et al., "Measurement and modeling of infrared imaging systems at conditions of reduced visibility (fog) for traffic applications," *Proc. SPIE* **2223**, 175–186 (1994).
12. J. Dumoulin and V. Boucher, "Infrared thermography system for transport infrastructures survey with inline local atmospheric parameter measurements and offline model for radiation attenuation evaluations," *Proc. SPIE* **8**(1), 084978 (2014).
13. M. T. Eismann and D. A. LeMaster, "Aerosol modulation transfer function model for passive long-range imaging over a nonuniform atmospheric path," *Opt. Eng.* **52**(4), 046201 (2013).
14. R. Nebuloni, "Empirical relationships between extinction coefficient and visibility in fog," *Appl. Opt.* **44**(18), 3795–3804 (2005).
15. I. Gultepe et al., "Ice fog in arctic during FRAM-ice fog project: aviation and nowcasting applications," *Bull. Am. Meteorolog. Soc.* **95**(2), 211–226 (2014).
16. I. Gultepe, M. D. Müller, and Z. Boybeyi, "A new visibility parameterization for warm-fog applications in numerical weather prediction models," *J. Appl. Meteorol. Climatol.* **45**(11), 1469–1480 (2006).
17. B. Ben-Dor et al., "Cloud, fog, and aerosol effect on the MTF of optical systems," *Proc. SPIE* **2580**, 9 (1995).
18. N. S. Kopeika, A. Zilberman, and Y. Yitzhaky, "Aerosol MTF revisited," *Proc. SPIE* **9071**, 907119 (2014).
19. C. D. Packard et al., "Measurement of optical blurring in a turbulent cloud chamber," *Proc. SPIE* **10002**, 100020E (2016).
20. S. Shamriz et al., "Prediction of overall atmospheric MTF with standard weather parameters: comparison with measurements with two imaging systems," *Proc. SPIE* **2471**, 13 (1995).
21. B. Ben Dor et al., "Atmospheric scattering effect on spatial resolution of imaging systems," *J. Opt. Soc. Am. A* **14**(6), 1329–1337 (1997).
22. L. R. Bissonnette, "Imaging through fog and rain," *Proc. SPIE* **31**(5), 8 (1992).
23. B. L. W. Gabriel et al., "Image quality, meteorological optical range, and fog particulate number evaluation using the Sandia National Laboratories fog chamber," *Opt. Eng.* **56**(8), 085104 (2017).
24. D. Sadot et al., "Restoration of thermal images distorted by the atmosphere, based on measured and theoretical atmospheric modulation transfer function," *Proc. SPIE* **33**(1), 10 (1994).
25. J. D. van der Laan et al., "Optical characterization of the Sandia fog facility," *Proc. SPIE* **10197**, 1019704 (2017).
26. J. D. van der Laan et al., "Superior signal persistence of circularly polarized light in polydisperse, real-world fog environments," *Appl. Opt.* **57**(19), 5464–5473 (2018).
27. Malvern Instruments, *Spraytec User Manual*, Malvern Instruments Ltd., Worcestershire, United Kingdom (2007).
28. World Meteorological Organization, *Guide to Meteorological instruments and Methods of Observation*, p. 681, Publications Board World Meteorological Organization, Geneva, Switzerland (2008).
29. M. Chaker, C. B. Meher-Homji, and I. I. I. T. Mee, "Inlet fogging of gas turbine engines: part b—fog droplet sizing analysis, nozzle types, measurement and testing," *Proc. SPIE* **36096**, 429–441 (2002).
30. E. P. Shettle and R. W. Fenn, "Models for the aerosols of the lower atmosphere and the effects of humidity variations on their optical properties," *Air Force Geophys. Lab Hanscom Afb Ma* (1979).
31. J. W. Goodman, *Introduction to Fourier Optics*, Roberts and Company Publishers, Greenwood Village, Colorado (2005).
32. G. C. Holst, *Testing and Evaluation of Infrared Imaging Systems*, JCD Pub., Winter Park, Florida (1998).
33. A. P. Tzannes and J. M. Mooney, "Measurement of the modulation transfer function of infrared cameras," *Proc. SPIE* **34**(6), 10 (1995).

Brian J. Redman received his BS degree in electrical engineering from Montana State University in 2014. He is working as an intern at Sandia National Laboratories. He is a graduate student of the College of Optical Sciences at the University of Arizona. His current research interests include long-wavelength infrared imaging, polarization, and channeled imaging systems. He is a member of SPIE.

John D. van der Laan received his BS degree in electrical engineering from Michigan Technological University and his MS and PhD degrees in optical sciences from the University of Arizona. His doctoral dissertation investigated polarized light transport through highly scattering environments and is titled "Evolution and persistence of circular and linear polarization in scattering environments." Currently, he is a senior member of technical staff at Sandia National Laboratories in the Advanced Remote Sensing Group.

Karl R. Westlake received his BS degree in electrical engineering from the University of New Mexico in 2007. He is a principal technologist at Sandia National Laboratories, Albuquerque, New Mexico, USA.

Jacob W. Segal received his BS degree in optical sciences and engineering from the University of Arizona in 2015. He is a senior optical technologist at Sandia National Laboratories.

Charles F. LaCasse received his PhD from the College of Optical Sciences at the University of Arizona in 2013. He is a senior member of technical staff at Sandia National Laboratories with expertise in polarization, innovative remote sensing concepts, and hyperspectral data 260 exploitations. He is a member of SPIE.

Andres L. Sanchez received his BS and MS degrees in chemical engineering and his MBA in management of technology from the University of New Mexico in 2008, 2012, and 2014, respectively. Currently, he is a senior member of technical staff at Sandia National Laboratories in WMD Threats and Aerosol Science. He has 9 years of expertise in aerosol science.

Jeremy B. Wright received his BS, MS, and PhD degrees in electrical engineering from the University of New Mexico, in 2007, 2010, and 2014, respectively. Currently, he is a senior member of technical staff at Sandia National Laboratories in the Tactical Sciences R&D Group performing research on optical systems. He is a member of SPIE.